ACS Biomaterials SCIENCE & ENGINEERING

pubs.acs.org/journal/abseba

Article

Intracellular Cargo Delivery Induced by Irradiating Polymer Substrates with Nanosecond-Pulsed Lasers

Weilu Shen, Stefan Kalies, Marinna Madrid, Alexander Heisterkamp, and Eric Mazur*

Cite This: *ACS Biomater. Sci. Eng.* 2021, 7, 5129–5134

Read Online

ACCESS | Metrics & More | Article Recommendations | Supporting Information

ABSTRACT: There is a great need in the biomedical field to efficiently, and cost-effectively, deliver membrane-impermeable molecules into the cellular cytoplasm. However, the cell membrane is a selectively permeable barrier, and large molecules often cannot pass through the phospholipid bilayer. We show that nanosecond laser-activated polymer surfaces of commercial polyvinyl tape and black polystyrene Petri dishes can transiently permeabilize cells for high-throughput, diverse cargo delivery of sizes of up to 150 kDa. The polymer surfaces are biocompatible and support normal cell growth of adherent cells. We determine the optimal irradiation conditions for poration, influx of fluorescent molecules into the cell, and post-treatment viability of the cells. The simple and low-cost substrates we use have no thin-metal structures, do not require cleanroom fabrication, and provide spatial selectivity and scalability for biomedical applications.

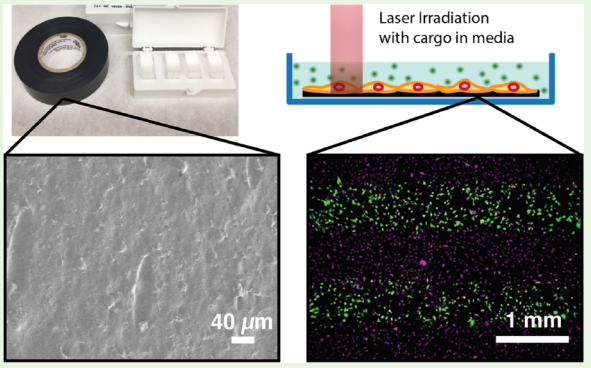

KEYWORDS: *spatially selective delivery, polymer, intracellular delivery, pulsed laser, metal oxide, carbon black*

INTRODUCTION

To advance basic research in medical biology and develop therapeutics, it is vital to understand and fix mechanisms at the cellular level[1] and manipulate biological functions through the delivery of molecular cargoes, such as proteins, antibodies, and genetic materials.[2,3] Proteins can be delivered into the cytosol to directly interfere with metabolic and signaling pathways of cells. Genetic materials such as small interfering RNA can be deployed to manipulate gene expression.[4] With the development of CRISPR-cas9, gene-editing can be used for gene-therapy treatments, such as CCR5-knockdown for HIV treatments.[5−10] In the emerging field of nanomedicine, it is important to deliver biologically interesting cargo and molecules directly into cells.[11,12] However, direct delivery of such cargoes into the cellular cytoplasm is a challenge.[13,14] Each of the existing intracellular delivery techniques, such as electroporation, viral transduction, and encapsulation with liposomal reagents, comes with strengths and weaknesses. While these methods may fit some application needs, they are hindered by problems such as toxicity, low efficiency, or low throughput. Another method, optotransfection,[15−17] provides high transfection efficiency, as well as high viability and selectivity, but has a very low throughput as it only transfects one cell at a time. To target and fix diseases, a cargo delivery platform must be able to perform with high efficiency and throughput without sacrificing cell viability.[18]

Nanotechnology and microfabrication have opened the door for the creation of devices on the scale of biological systems.[19] Many devices have been created for cargo delivery, including devices that use squeezing as the physical mechanism,[20] microcapillary pipettes for microinjecting cargo,[21] microfluidic devices,[22] and plasmonic materials for cell poration. Plasmonic poration of cells has been demonstrated using metallic nanoparticles[23] and a variety of substrates made of titanium nitride, gold, and titanium, such as pyramidal arrays fabricated using photolithography and nanocavity structures fabricated using self-assembling colloids;[24−28] however, metals used in nanophotothermolysis can fragment.[29] To avoid the risk of metallic fragmentation from thin films and nanoparticles, it is important to explore other nonmetallic thin-film materials. Nonmetallic particles such as carbon nanoparticles[30] and polydopamine nanosensitizer particles[31] have been designed and synthesized for efficient cargo delivery, and this demonstrates that carbon particles and polymer particles can be used in place of metallic particles that have been traditionally used for targeted drug delivery. The development of nonmetallic particles has also opened doors to nonmetallic substrate systems as delivery devices.

Received: May 17, 2021
Accepted: August 17, 2021
Published: October 4, 2021

https://doi.org/10.1021/acsbiomaterials.1c00656
ACS Biomater. Sci. Eng. 2021, 7, 5129−5134

In this paper, we demonstrate the use of polymer substrates for cell poration and cargo delivery. We use commercially available polyvinyl tape and black polystyrene Petri dishes to deliver fluorescent cargo to cells and measure the post-delivery viability of the cells. The polymer substrates are nontoxic to cell lines and support normal cell growth and adhesion for adherent cells. We use a near-infrared laser to minimize interference with biological processes in the cells.[32] By raster scanning the laser beam over the substrates, we are able to deliver cargo to cells at a rate of about 50,000 cells/min. We demonstrate delivery of fluorescent dye molecules, ranging from 648 Da to 150 kDa to adherent cell lines, and determine the optimal irradiation parameters for delivery of these molecules; for calcein green (648 Da), we achieve delivery efficiencies of up to 40% with viabilities of 60%. Our results demonstrate cargo delivery by nanosecond-pulsed laser irradiation of off-the-self polymer, obviating the need for nanofabrication and costly materials. While free-flowing particle systems may require complicated chemical synthesis or functionalization techniques, our method, which utilizes bulk substrates, does not. Using bulk polymer substrates opens the door to readily molded structures such as scaffolds for different biological applications.

EXPERIMENTAL SECTION

Our substrate is pigmented polyvinyl on a glass coverslip, as shown in Figure 1a. Off-the-shelf black and white polyvinyl Duck Brand

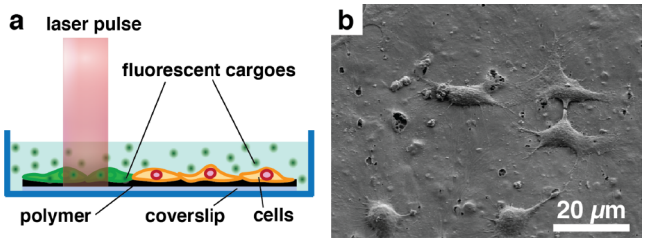

Figure 1. (a) Schematic of the polymer-based cargo delivery setup. Cells are seeded on a polymer substrate placed inside a Petri dish filled with a fluorescent cargo-containing medium. Laser energy absorbed by the polymer substrate results in transient pores in the cellular membrane, allowing the cargo to diffuse into the cells. (b) Scanning electron microscopy image of HeLa cells fixed on a carbon black-pigmented polyvinyl surface, showing cell adherence and material surface morphology. The cells are rounded features of about 15 μm size.

Professional Electrical Tape substrates are used and mounted on glass no. 2 coverslips, adhesive-side down, for rigidity and ease of handling. These substrates are placed in a 100 mm Petri dish for cell seeding. We grow adherent HeLa CCL-2 or Panc-1 cells on the substrates in a mixture of 10% fetal bovine serum medium, Dulbecco's modified Eagle's medium without phenol red, 1% L-glutamine, and 1% penicillin streptomycin. The samples are incubated at 37 °C and 5% CO_2 and passaged two to three times per week. The cells are used in experiments when they reach 80% confluence in flasks and before the 30th passage. Five million cells are seeded overnight in 15 mL of medium in a 100 mm Petri dish. After the cells are grown on the substrates, each seeded substrate is transferred from the media-filled 100 mm Petri dish to a 35 mm Petri dish with 2 mL of a phosphate buffered saline (PBS) solution. The solution contains the membrane-impermeable fluorescent cargo of interest: calcein green at 0.57 mg/mL or FITC-dextran (10, 20, 40, 70, and 150 kDa-sized) at 25 mg/mL. When the cell membrane is porated, the membrane-impermeable dye molecules diffuse into the cytoplasm before the pores close. The loaded cells are detected in the green fluorescence channel. Figure 1b shows HeLa cells that are chemically fixed on the polymer substrates, with a 5 nm thick coating of Pt/Pd to permit scanning electron microscopy. The cells adhere to the sample surface without any surface treatment.

The dish with the seeded samples is placed on an *xy* scanning stage to permit raster scanning of the laser beam over a selected area of the sample. The system uses an 11 ns pulsed Nd:YAG (neodymium-doped yttrium aluminum garnet) laser with a repetition rate of 50 Hz, operating at a wavelength of 1064 nm, and is Q-switched and turn-key operated. The diameter of the laser beam spot on the substrate surface is approximately 1 mm and has a Gaussian beam profile. The energy output of the laser is varied using a built-in laser attenuator and a half-wave plate and polarizer combination, yielding an excitation fluence ranging from 30 to 130 mJ/cm^2 at the substrate surface. The scanning-stage raster scans the sample in the *x* and *y* directions over a distance of 100 mm and 500 μm, respectively, at a speed of 10 mm/s. Given this speed, laser repetition rate, and the laser beam spot size, each point in the scanned area is exposed to about six laser pulses.

To determine the viability of the cells post-treatment, we transfer the cell-covered substrate to a new 36 mm Petri dish, incubate the cells for 15 min in a solution containing 2 mL of calcein AM red-orange (emission at 590 nm under 577 nm excitation), a viability indicator, and then rinse them twice in PBS. After acetoxymethyl ester hydrolysis of calcein AM red-orange by intracellular esterase, only cells with healthy metabolic activity express fluorescence in the red channel. Cells that express calcein AM red-orange and the delivery cargo in the green channel (emission at 515 nm under 495 nm excitation) are both alive and have the non-membrane-permeable cargo delivered into the cytoplasm before the pores close. The ability to perform spatial selectivity of treatment allows for *in situ* control experiments in the same Petri dish.

To quantify the treatment efficiency and viability for each experiment, we take two images of each area that has been irradiated: one in the green channel to determine the efficiency of delivery and one in the red channel to determine viability. The images are overlaid and processed in ImageJ to count the number of cells in each channel in the selected area. Efficiency and viability are determined by dividing the number of green-emitting and red-emitting cells, respectively, by the number of red-emitting cells in an equally sized control area that is not irradiated. Each experiment is repeated three times to obtain the standard error from three independent experiments.

RESULTS

Figure 2 shows the fluence dependence of the calcein-green delivery efficiency and post-treatment viability of HeLa CCL2 and Panc-1 cells grown on a black polyvinyl substrate. The post-treatment viability decreases with increasing fluence because the increased radiation causes the cells to lyse and so they can no longer hold the cargo inside. Although the delivery efficiency initially increases with increasing fluence, it is capped by viability and therefore decreases at high fluence. For both cell types, we obtain a maximum calcein-green delivery efficiency of 40% and a viability of 60% at a fluence of 76 mJ/cm^2.

To study the feasibility of larger cargo, we also studied the delivery of 10, 20, and 40 kDa FITC-dextran molecules to HeLa cells in a black polyvinyl sample. Figure 3 shows the green (left) and red (right) fluorescent images and integrated intensity profiles from the samples after irradiation, showing delivery and viability, respectively. The bright bands in the left images correspond to the regions where cargo was delivered to the cells; in each of the images, the top band was irradiated at a fluence of 89 mJ/cm^2 and the bottom one at 76 mJ/cm^2. The dark regions around these bands correspond to regions that were not irradiated and where no cargo was delivered to the cells. Note that the fluorescence intensity is higher at the higher irradiation fluence and that it decreases with increasing

https://doi.org/10.1021/acsbiomaterials.1c00656
ACS Biomater. Sci. Eng. 2021, 7, 5129−5134

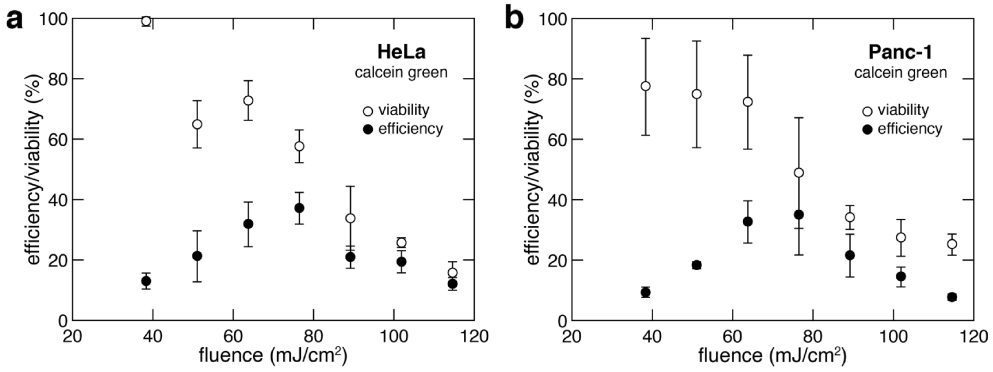

Figure 2. Fluence dependence of the viability (open circles) and delivery efficiency (closed circles) of calcein green delivery to (a) HeLa and (b) Panc-1 cells. Viability is defined as the number of cells that express calcein AM red-orange (a viability indicator) in a laser-scanned area divided by those in an equal-sized non-laser-scanned area. Efficiency is defined as the number of cells that show fluorescence in the green channel divided by the number of cells that express calcein AM red-orange in an equal-sized non-laser-scanned area. The mean efficiency and viability with corresponding error bars denoting standard error from $n = 3$ independent experiments are plotted.

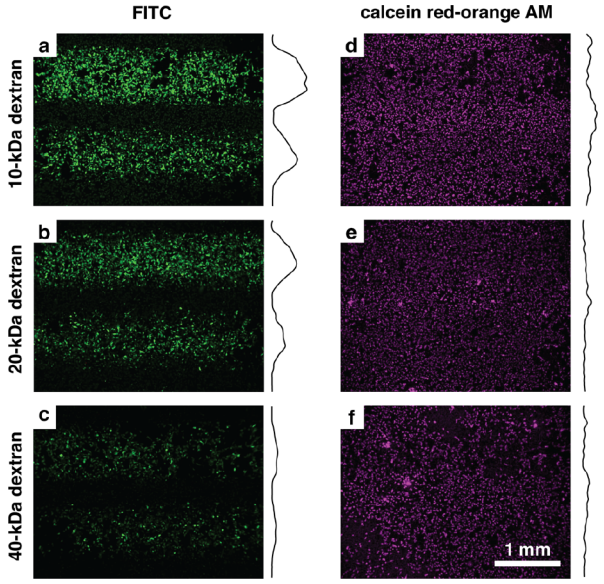

Figure 3. Delivery efficiency and viability of delivery of dextran molecules of various molecular weights to HeLa cells using nanosecond laser irradiation of a black vinyl polymer surface. Expression of FITC-dextran of molecular weights (a) 10 kDa, (b) 20 kDa, and (c) 40 kDa in HeLa cells. (d–f) Corresponding viability post-treatment with calcein AM red-orange (images altered to magenta for color-differentiation clarity). The top strips in each image were exposed to a fluence of 89 mJ/cm^2 and the bottom strips to 76 mJ/cm^2. The curves to the right of each image represent the horizontally integrated intensity across the image.

cargo size. The corresponding fluorescent images on the right show that there is little cell death at these fluences. The Supporting Information provides a quantitative measurement, using flow cytometry, of delivery efficiency and viability for larger FITC-dextran cargoes: we were able to achieve ∼40% delivery efficiency for 10 and 20 kDa molecules and ∼20% for 40, 70, and 150 kDa molecules. It should be noted that we do not observe cargo delivery on clear polyvinyl tape, on a clear polystyrene Petri dish, or on a clear glass coverslip, suggesting that pigments that interact with the laser wavelength are required for delivery.

The laser-irradiated black tape can also support primary cell growth, as demonstrated in the Supporting Information. Calcein green and dextran 10 kDa were delivered to primary human aortic valve interstitial cells. We were also able to deliver FAM-labeled Negative Control No. 1 siRNA (Silencer from Invitrogen) to HeLa cells at a rate of 9.2% with the black polyvinyl tape, as shown in the flow cytometry measurements in the Supporting Information. This is much lower than the 40% delivery efficiency that we were able to achieve with the FITC-dextran 10 kDa molecules. This may be due to the lower concentration of the siRNA molecules in the media during irradiation.

We also investigated cargo delivery on black polystyrene (Supporting Information) and white polyvinyl samples (Figure 4). Black polymers are pigmented with carbon black, whereas white polymers are pigmented with a metal oxide, such as titanium dioxide or zinc oxide.[33] We directly seeded HeLa cells on a black polystyrene Petri dish, while the white polyvinyl samples were placed in a regular Petri dish, seeded with HeLa cells. The white polyvinyl samples scatter the incident light, which causes a background signal in the images. As shown in Figure 4, the green fluorescence images show two bands, corresponding to the areas irradiated by the laser. For the white polyvinyl, we used fluences of 130 mJ/cm^2 (top band) and 120 mJ/cm^2 (bottom band). The images demonstrate that we also can deliver cargo to HeLa cells using white polyvinyl and black polystyrene. A higher range of laser fluence was used for the white polyvinyl than for the black polyvinyl, as lower laser fluence irradiation does not produce porated cells on the white polyvinyl substrates.

The polymer substrates vary greatly in optical absorption. Table 1 shows the spectrophotometer measurements of white polyvinyl and black polyvinyl, indicating high absorptance at 1064 nm for black polyvinyl and low absorptance at this wavelength for white polyvinyl and showing that delivery and absorption of energy are not correlated. A previous study, however, reports a relationship between impulse and laser-induced or shock-wave-induced cargo delivery to cells.[34] To monitor any acoustic wave generated by the laser irradiation of the samples, we measured the pressure near the irradiated area (Supporting Information). As one would expect, the amplitude of the pressure wave correlates with absorption. However, it does not correlate with cargo delivery, as we observe no pressure waves for white polyvinyl, which delivers cargo as efficiently as the black polyvinyl.

https://doi.org/10.1021/acsbiomaterials.1c00656
ACS Biomater. Sci. Eng. 2021, 7, 5129–5134

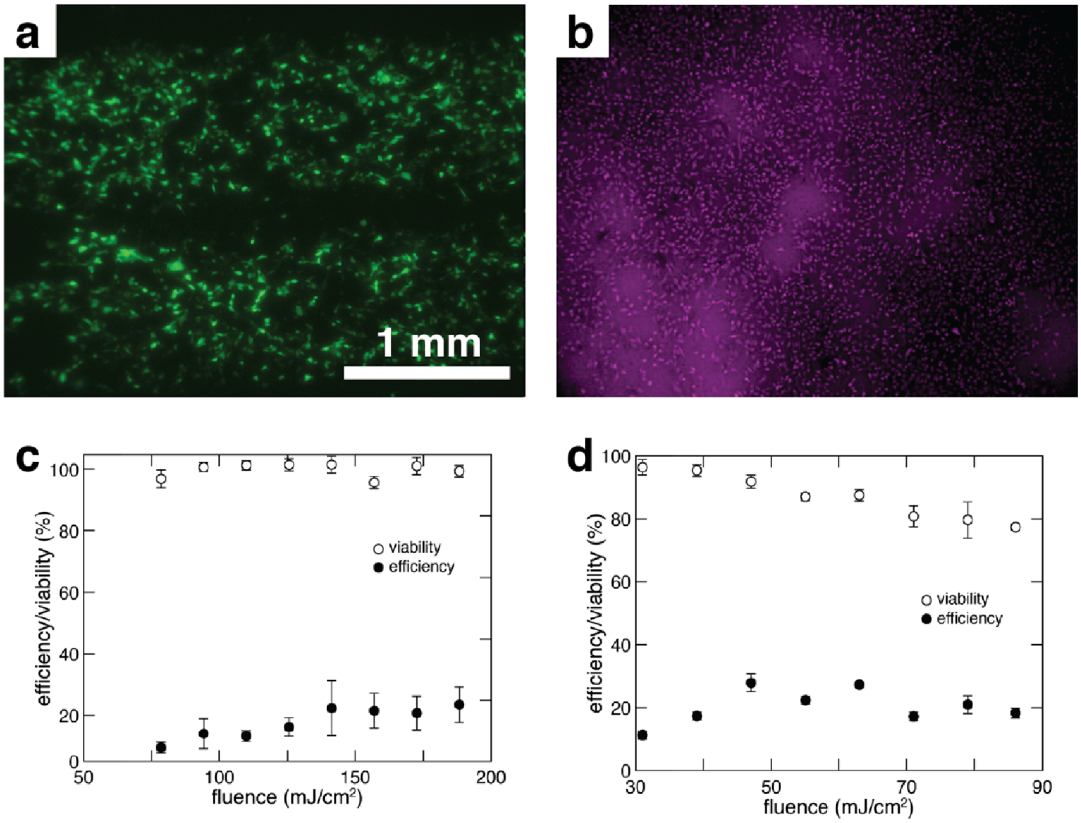

Figure 4. (a) HeLa cells with calcein green and (b) the same cells stained with a viability indicator, calcein AM red-orange (images altered to magenta for color-differentiation clarity). (c) Measurement of delivery efficiency and viability of calcein green at varying laser fluences, quantified by flow cytometry, with white polyvinyl tape substrates and (d) black polyvinyl tape substrates. Viability is obtained using propidium iodide to stain dead cells. The mean efficiency and viability with corresponding error bars denoting standard error from $n = 3$ independent experiments (flow cytometry measurements for each experiment account for 10,000 cells) are plotted.

Table 1. Spectrophotometer Measurements of the White Polyvinyl Tape, Black Polyvinyl Tape, and Black Polystyrene Petri Dish at 1064 nm Wavelength[a]

	R	T	$A = 1 - R - T$
white tape	0.628	0.385	0.013
black tape	0.043		0.957
black Petri dish	0.054	−0.001	0.947

[a]The reflectance and transmission are measured directly from the samples, and the absorption is calculated and obtained as 1 minus the reflection and transmission. No transmission is measured from the black tape.

DISCUSSION

Our results conclusively show that we can deliver cargo to cells using a variety of polymer surfaces. We demonstrate delivery of cargo up to 150 kDa, which is on the scale of siRNA and CRISPR-cas9, and obtain efficiencies and viabilities approaching those obtained with nanofabricated gold pyramids,[24] titanium-nitride inverse pyramids,[26] and self-assembled titanium nanocavities,[27] which were also irradiated with the same pulsed-laser wavelength and parameters. The viability at maximum efficiency we obtain for the delivery of calcein green to HeLa cells on off-the-shelf polymer substrates (60%) is lower than the viability obtained for the metallic nanostructured substrates (87−98%) and requires a higher laser fluence (7.5 mJ/cm^2 vs 1−5 mJ/cm^2). Similarly, the maximum efficiency on the polymer substrates (40%) is lower than that for metallic nanostructured substrates (78−95%), but part of this decrease in efficiency is due to the lower viability.

While it may be possible to improve the efficiency by optimizing the surface morphology of the polymer substrates, the simplicity of these materials makes them appealing even if the performance is somewhat diminished compared to other techniques. Polymer substrates are inexpensive and could be easily integrated into devices. Unlike the nanostructured substrates, polymer substrates involve no metals and do not require nanofabrication or clean-room handling. However, polymer structures may be combined with metals such as gold to fabricate a controlled heating substrate for efficient cargo delivery of around 90% in the kilo-dalton-sized range.[35] Dynamic photothermal polymers have also been synthesized and functionalized to harness localized heating to perform transfection of 100 kDa sized genetic materials at around 85% efficiency,[36] further motivating nonreliance of thin-film metal structures for efficient cell-membrane poration and to lower the cost of device production.

Laser-irradiated delivery of cargo to cells relies on diffusion through transient pores that are formed in the cell membrane during laser irradiation.[16] The larger the cargo, the lower the probability that it will enter the cellular cytoplasm via the transient pores before they self-heal. Indeed, the deliver efficiency decreases with cargo size, both for the polymer substrates (Figure 3) and for the nanofabricated gold pyramids.[24]

Previous work on cargo delivery with laser-irradiated metallic substrates involved nanostructured surfaces. The

https://doi.org/10.1021/acsbiomaterials.1c00656
ACS Biomater. Sci. Eng. 2021, 7, 5129−5134

polymer substrates, however, have a very different surface morphology from the nanostructured substrates. Scanning electron microscopy reveals random structures over a range of sizes, while profilometry shows that the surface roughness is around 1 μm (see the Supporting Information). The surface roughness increases slightly after irradiation with fluences for which the viability decreases. In the scope of pulsed-laser-irradiated substrate-based platforms, between the polymer substrates and metallic substrates and particles from previous reports in the literature, there appears to be no correlation between surface features and poration.

Polyvinyl chloride begins to deform at around 170−180 °C,[37] which suggests that the black polyvinyl tape substrates reach these temperatures at high laser-fluence irradiation; however, the surface roughness does not change even at higher fluences for the white polyvinyl substrate. The lack of pressure waves measured from irradiated white polyvinyl and the low absorption at 1064 nm in the spectrophotometer point to the absence of a high temperature rise for the poration method. High-absorbent and low-absorbent substrates both cause cargo delivery upon laser irradiation. The higher viability attained in the flow cytometry measurements for the white polyvinyl tape compared to the black polyvinyl tape suggests laser-irradiating inert metal oxides may prevent post-treatment cell death. The laser−material interactions between nanosecond pulsed laser and metal oxides, such as titanium dioxide, may be further explored in the future.

CONCLUSIONS

We demonstrated direct intracellular cargo delivery using simple, off-the-shelf polymer substrates and a turn-key pulsed laser, which permits spatially selective cargo delivery within a population of cells. Even without optimization of the substrates, the delivery method with absorbent black polyvinyl surfaces is effective for cargo up to 150 kDa in mass, opening the door to the delivery of small genetic molecules using very simple and inexpensive means. The spatial selectivity of the method allows for *in situ* control experiments in a single Petri dish, with cargo delivered only to selected regions in the dish. The simple method also opens the door for a more sophisticated design incorporating inert oxides such as titanium dioxide and for further investigation on controlled perturbation of the cell membrane.

Because polymers are readily molded into scaffolds, the technique we present can support direct intracellular cargo delivery for different biological and biomedical applications. Some polymers, such as bioplastics using agarose or chitosan, are both biocompatible and biodegradable. These polymers can be combined with pulsed-laser systems to create potential *in vitro* cell treatments. The combination of biocompatible, and possibly biodegradable, polymers and pulsed-laser excitation creates a simple and versatile intracellular delivery platform that paves the way for new research and treatments in cell biology and medicine.

ASSOCIATED CONTENT

Supporting Information

The Supporting Information is available free of charge at https://pubs.acs.org/doi/10.1021/acsbiomaterials.1c00656.

Optical profilometer measurement of surface roughness of black polyvinyl surfaces after being exposed to lasers of varying fluences; SEM images of substrates pre- and post-laser irradiation; needle hydrophone measurements of pressure wave impulse with respect to laser fluence and calculation details; sets of flow cytometer measurement plots and raw data; and sets of raw fluorescence images of cells on substrates treated by laser irradiation (PDF)

AUTHOR INFORMATION

Corresponding Author

Eric Mazur − *John A. Paulson School of Engineering and Applied Sciences, Harvard University, Cambridge, Massachusetts 02138, United States; Department of Physics, Harvard University, Cambridge, Massachusetts 02138, United States;* orcid.org/0000-0003-3194-9836; Email: mazur@seas.harvard.edu

Authors

Weilu Shen − *John A. Paulson School of Engineering and Applied Sciences, Harvard University, Cambridge, Massachusetts 02138, United States;* orcid.org/0000-0002-6850-4972

Stefan Kalies − *Institut für Quantenoptik, Gottfried Wilhelm Leibniz Universität Hannover, 30167 Hannover, Germany; Lower Saxony Centre for Biomedical Engineering, Implant Research and Development, 30625 Hannover, Germany*

Marinna Madrid − *John A. Paulson School of Engineering and Applied Sciences, Harvard University, Cambridge, Massachusetts 02138, United States;* orcid.org/0000-0002-4305-8099

Alexander Heisterkamp − *Institut für Quantenoptik, Gottfried Wilhelm Leibniz Universität Hannover, 30167 Hannover, Germany; Lower Saxony Centre for Biomedical Engineering, Implant Research and Development, 30625 Hannover, Germany*

Complete contact information is available at: https://pubs.acs.org/10.1021/acsbiomaterials.1c00656

Author Contributions

W.S. conceived the basic idea for this work. W.S. designed and carried out the experiments and analyzed and interpreted the results. S.K. analyzed and interpreted the results. M.M. prepared samples for scanning electron microscopy and interpreted the results. E.M. and A.H. supervised the research and the development of the manuscript. W.S. wrote the first draft of the manuscript; all authors subsequently took part in the revision process and approved the final copy of the manuscript

Funding

The research described in this paper was supported by National Science Foundation under contracts PHY-1219334 and PHY-1806434. This work was performed in part at the Harvard University Center for Nanoscale Systems (CNS), a member of the National Nanotechnology Coordinated Infrastructure Network (NNCI), which is supported by the National Science Foundation under NSF award numbers ECCS-1541959 and ECCS-2025158. W.S. was funded by the Smith Family Graduate Science and Engineering Fellowship at Harvard University.

Notes

The authors declare the following competing financial interest(s): In accordance with ACS policy and our ethical obligations as researchers, Marinna Madrid reports an interest

in Cellino Biotech, Inc., a company that may be affected by the research reported in the enclosed paper. Marinna Madrid discloses these interests fully to ACS and agrees to manage any potential conflicts arising from said involvement. The other authors declare no conflict of interest.

■ ACKNOWLEDGMENTS

Several people contributed to the work described in this paper. The authors thank Alex Raymond for discussions and help on the hydrophone setup, Sarah Camayd-Muñoz for discussions, Arthur McClelland for discussions, and Zachary Niziolek for help with the flow cytometer.

■ REFERENCES

(1) Wagner, V.; Dullaart, A.; Bock, A.; Zweck, A. The Emerging Nanomedicine Landscape. *Nat. Biotechnol.* **2006**, *24*, 1211−1217.
(2) Langer, R. New Methods of Drug Delivery. *Science* **1990**, *249*, 1527−1533.
(3) Marx, V. Cell Biology: Delivering Tough Cargo into Cells. *Nat. Methods* **2016**, *13*, 37−40.
(4) Shegokar, R.; Shaal, L. A. L.; Mishra, P. R. SiRNA Delivery: Challenges and Role of Carrier Systems. *Pharmazie* **2011**, *66*, 313−318.
(5) Wang, X.; Huang, X.; Fang, X.; Zhang, Y.; Wang, W. CRISPR-Cas9 System as a Versatile Tool for Genome Engineering in Human Cells. *Mol. Ther.—Nucleic Acids* **2016**, *5*, No. e388.
(6) Somia, N.; Verma, I. M. Gene Therapy: Trials and Tribulations. *Nat. Rev. Genet.* **2000**, *1*, 91−99.
(7) Phillips, A. J. The Challenge of Gene Therapy and DNA Delivery. *J. Pharm. Pharmacol.* **2001**, *53*, 1169−1174.
(8) Steinberger, P.; Andris-Widhopf, J.; Bühler, B.; Torbett, B. E.; Barbas, C. F. Functional Deletion of the CCR5 Receptor by Intracellular Immunization Produces Cells That Are Refractory to CCR5-Dependent HIV-1 Infection and Cell Fusion. *Proc. Natl. Acad. Sci. U. S. A.* **2000**, *97*, 805−810.
(9) Patil, S. D.; Rhodes, D. G.; Burgess, D. J. DNA-Based Therapeutics and DNA Delivery Systems: A Comprehensive Review. *AAPS J* **2005**, *7*, E61−E77.
(10) Xu, L.; Yang, H.; Gao, Y.; Chen, Z.; Xie, L.; Liu, Y.; Liu, Y.; Wang, X.; Li, H.; Lai, W.; He, Y.; Yao, A.; Ma, L.; Shao, Y.; Zhang, B.; Wang, C.; Chen, H.; Deng, H. CRISPR/Cas9-Mediated CCR5 Ablation in Human Hematopoietic Stem/Progenitor Cells Confers HIV-1 Resistance In Vivo. *Mol. Ther.* **2017**, *25*, 1782−1789.
(11) Langer, R. Drug Delivery and Targeting. *Nature* **1998**, *392*, 5−10.
(12) Kim, B. Y. S.; Rutka, J. T.; Chan, W. C. W. Nanomedicine. *N. Engl. J. Med.* **2010**, *363*, 2434−2443.
(13) Sanhai, W. R.; Sakamoto, J. H.; Canady, R.; Ferrari, M. Seven Challenges for Nanomedicine. *Nat. Nanotechnol.* **2008**, *3*, 242−244.
(14) Chauhan, V. P.; Jain, R. K. Strategies for Advancing Cancer Nanomedicine. *Nat. Mater.* **2013**, *12*, 958−962.
(15) Tirlapur, U. K.; König, K. Cell Biology: Targeted Transfection by Femtosecond Laser. *Nature* **2002**, *418*, 290−291.
(16) Davis, A. A.; Farrar, M. J.; Nishimura, N.; Jin, M. M.; Schaffer, C. B. Optoporation and Genetic Manipulation of Cells Using Femtosecond Laser Pulses. *Biophys. J.* **2013**, *105*, 862−871.
(17) Soman, P.; Zhang, W.; Umeda, A.; Zhang, Z. J.; Chen, S. Femtosecond Laser-Assisted Optoporation for Drug and Gene Delivery into Single Mammalian Cells. *J. Biomed. Nanotechnol.* **2011**, *7*, 334−341.
(18) Stewart, M. P.; Langer, R.; Jensen, K. F. Intracellular Delivery by Membrane Disruption: Mechanisms, Strategies, and Concepts. *Chem. Rev.* **2018**, *118*, 7409−7531.
(19) Wu, Y.-C.; Wu, T.-H.; Clemens, D. L.; Lee, B.-Y.; Wen, X.; Horwitz, M. A.; Teitell, M. A.; Chiou, P.-Y. Massively Parallel Delivery of Large Cargo into Mammalian Cells with Light Pulses. *Nat. Methods* **2015**, *12*, 439−444.
(20) Sharei, A.; Zoldan, J.; Adamo, A.; Sim, W. Y.; Cho, N.; Jackson, E.; Mao, S.; Schneider, S.; Han, M.-J.; Lytton-Jean, A.; Basto, P. A.; Jhunjhunwala, S.; Lee, J.; Heller, D. A.; Kang, J. W.; Hartoularos, G. C.; Kim, K.-S.; Anderson, D. G.; Langer, R.; Jensen, K. F. A Vector-Free Microfluidic Platform for Intracellular Delivery. *Proc. Natl. Acad. Sci. U. S. A.* **2013**, *110*, 2082−2087.
(21) Cottle, R. N.; Lee, C. M.; Archer, D.; Bao, G. Controlled Delivery of β-Globin-Targeting TALENs and CRISPR/Cas9 into Mammalian Cells for Genome Editing Using Microinjection. *Sci. Rep.* **2015**, *5*, No. 16031.
(22) Kim, J.; Hwang, I.; Britain, D.; Chung, T. D.; Sun, Y.; Kim, D.-H. Microfluidic Approaches for Gene Delivery and Gene Therapy. *Lab Chip* **2011**, *11*, No. 3941.
(23) Lachaine, R.; Etienne Boulais, M. M. From Thermo- to Plasma-Mediated Ultrafast Laser-Induced Plasmonic Nanobubbles. *ACS Photonics* **2013**, *1*, 331−336.
(24) Saklayen, N.; Huber, M.; Madrid, M.; Nuzzo, V.; Vulis, D. I.; Shen, W.; Nelson, J.; McClelland, A. A.; Heisterkamp, A.; Mazur, E. Intracellular Delivery Using Nanosecond-Laser Excitation of Large-Area Plasmonic Substrate. *ACS Nano* **2017**, *11*, 3671−3680.
(25) Saklayen, N.; Kalies, S.; Madrid, M.; Nuzzo, V.; Huber, M.; Shen, W.; Sinanan-Singh, J.; Heinemann, D.; Heisterkamp, A.; Mazur, E. Analysis of Poration-Induced Changes in Cells from Laser-Activated Plasmonic Substrates. *Biomed. Opt. Express* **2017**, *8*, 437−444.
(26) Raun, A.; Saklayen, N.; Zgrabik, C.; Shen, W.; Madrid, M.; Huber, M.; Hu, E.; Mazur, E. A Comparison of Inverted and Upright Laser-Activated Titanium Nitride Micropyramids for Intracellular Delivery. *Sci. Rep.* **2018**, *8*, No. 15595.
(27) Madrid, M.; Saklayen, N.; Shen, W.; Huber, M.; Vogel, N.; Mazur, E. Laser-Activated Self-Assembled Thermoplasmonic Nanocavity Substrates for Intracellular Delivery. *ACS Appl. Bio Mater.* **2018**, *1*, 1793−1799.
(28) Courvoisier, S.; Saklayen, N.; Huber, M.; Chen, J.; Diebold, E. D.; Bonacina, L.; Wolf, J. P.; Mazur, E. Plasmonic Tipless Pyramid Arrays for Cell Poration. *Nano Lett.* **2015**, *15*, 4461−4466.
(29) Pustovalov, V. K.; Smetannikov, A. S.; Zharov, V. P. Photothermal and Accompanied Phenomena of Selective Nanophotothermolysis with Gold Nanoparticles and Laser Pulses. *Laser Phys. Lett.* **2008**, *5*, 775−792.
(30) Sengupta, A.; Kelly, S. C.; Dwivedi, N.; Thadhani, N.; Prausnitz, M. R. Efficient Intracellular Delivery of Molecules with High Cell Viability Using Nanosecond-Pulsed Laser-Activated Carbon Nanoparticles. *ACS Nano* **2014**, *8*, 2889−2899.
(31) Harizaj, A.; Wels, M.; Raes, L.; Stremersch, S.; Goetgeluk, G.; Brans, T.; Vandekerckhove, B.; Sauvage, F.; De Smedt, S. C.; Lentacker, I.; Braeckmans, K. Photoporation with Biodegradable Polydopamine Nanosensitizers Enables Safe and Efficient Delivery of MRNA in Human T Cells. *Adv. Funct. Mater.* **2021**, *31*, No. 2102472.
(32) Strangman, G.; Boas, D. A.; Sutton, J. P. Non-Invasive Neuroimaging Using Near-Infrared Light. *Biol. Psychiatry* **2002**, *52*, 679−693.
(33) Pritchard, G. *Plastics Additives: An A-Z Reference*, Vol. *53*; Springer: Netherlands, 1998.
(34) Kodama, T.; Hamblin, M. R.; Doukas, A. G. Cytoplasmic Molecular Delivery with Shock Waves: Importance of Impulse. *Biophys. J.* **2000**, *79*, 1821−1832.
(35) Wu, J.; Zheng, Y.; Jiang, S.; Qu, Y.; Wei, T.; Zhan, W.; Wang, L.; Yu, Q.; Chen, H. Two-in-One Platform for High-Efficiency Intracellular Delivery and Cell Harvest: When a Photothermal Agent Meets a Thermoresponsive Polymer. *ACS Appl. Mater. Interfaces* **2019**, *11*, 12357−12366.
(36) Wang, J.; Ren, K. F.; Gao, Y. F.; Zhang, H.; Huang, W. P.; Qian, H. L.; Xu, Z. K.; Ji, J. Photothermal Spongy Film for Enhanced Surface-Mediated Transfection to Primary Cells. *ACS Appl. Bio Mater.* **2019**, *2*, 2676−2684.
(37) Patrick, S. *Practical Guide to Polyvinyl Chloride*; iSmithers Rapra Publishing, 2005.

https://doi.org/10.1021/acsbiomaterials.1c00656
ACS Biomater. Sci. Eng. 2021, 7, 5129−5134